Analyses of Teflon Surface Charring and Near Field Plume of a Micro-Pulsed Plasma Thruster

Michael Keidar and Iain D. Boyd

Department of Aerospace Engineering, University of Michigan, Ann Arbor MI 48109
734-764-7479, keidar@engin.umich.edu

Frank S. Gulczinski III, Erik L. Antonsen and Gregory G. Spanjers

Air Force Research Laboratory, Propulsion Directorate, Electric Propulsion Laboratory
Edwards AFB CA 93524

IEPC-01-155

The Teflon ablation in a micro-Pulsed Plasma Thruster is studied with an aim to understand the charring phenomena. Microscopic analysis of the charred areas shows that it contains mainly carbon. It is concluded that the carbon char is formed as result of carbon flux returned from the plasma. A simplified model of the current layer near the Teflon surface is developed. The current density and the Teflon surface temperature have peaks near the electrodes that explain preferential ablation of these areas as was observed experimentally. The comparison of the temperature field and the ablation rate distribution with photographs of the Teflon surface shows that the area with minimum surface temperature and ablation rate corresponds to the charring area. This suggests that the charring may be related to a temperature effect. Electron densities predicted by the plume model are compared with near field measurements.

Introduction

Pulsed plasma thrusters (PPT's) have been investigated since the early 1960's and were among the first of various electrical propulsion concepts accepted for space flight mainly due to their simplicity and hence high reliability[1]. However, the PPT has an efficiency at the low level of 10% (Ref. 2) and therefore several ways for improvement have been suggested[3]. Currently, PPT's are considered as an attractive propulsion option for stationkeeping and drag makeup purposes of mass and power limited satellites[4,5]. Recently, a micro-PPT has being designed at the Air Force Research Laboratory for delivery of very small impulse bit[6]. This is a simplified miniaturized version of a conventional PPT with a thrust in the 10 μN range designed to provide attitude control and stationkeeping for microsatellites.

Complete assessment of the spacecraft integration effects requires characterization of the plasma plume exhaust of a PPT. Previously we have developed an end-to-end model of the PPT and its plume with application to electrothermal[7,8] and electromagnetic PPT's[9]. It became clear that the plasma distribution in the plume field heavily depends upon upstream boundary conditions. Therefore the model of the plasma generation in these devices becomes a very important aspect of accurate plasma plume simulation.

In the present paper we will focus on the MicroPPT. Inspection of the micro-PPT propellant surface after firing indicated signs of charring and preferential ablation near the electrodes[6,10]. We present also results of the microscopic analyses of the charring areas that is the useful tool for understanding of the charring mechanism. In order to understand this phenomenon a model of the plasma layer near the Teflon surface is developed. In addition, the solution of the model will provide boundary conditions for the plasma plume.

Microscopic analyses of the Teflon surface

The AFRL MicroPPT in development for TechSat21 uses a 3 electrode configuration[6]. A small diameter rod (center electrode) is encased in a small-diameter annulus of Teflon, which is then encased in a relatively small diameter tube, which acts as the intermediate electrode. This construction is then encased in a second larger diameter annulus of Teflon, which is then encased in a large diameter outer electrode. The MicroPPT is fired by a low-energy breakdown between the intermediate and central electrode. This discharge provides enough seed ionization to enable the higher energy conduction breakdown between the intermediate and out electrodes. The discharge between the intermediate and central electrode is referred to as the trigger discharge. The discharge between the intermediate and outer electrode is referred to as the "main discharge". Although a wide range of parameters are tested in various MicroPPT configurations, typically the trigger discharge will consume about 1/50 the energy of main discharge. In this fashion, the MicroPPT has demonstrated the ability to passively initiated a surface breakdown discharge across outer propellant diameters as high as ¼" using a relatively low voltage below 3000V. Without the 3-electrode configuration, up to 40 kV would be required to initiate the discharge across a ¼" diameter. Requiring a 40 kV charge would place excessive design requirements on the power-processing unit and on the spacecraft EMI shielding.

In this work, research is performed on 2-electrode MicroPPT configurations. The discharge occurs between an inner cathode rod and an outer anode tube, across a Teflon annulus. Understanding the physical processes in this simplified geometry has proven beneficial in advancing the optimization of the MicroPPT by separating the requirements for the trigger and main discharges. Research[6,10] on small diameter 2-electrode designs, generally between 1-3 mm, is applicable to the trigger discharge. Research [6,11] on larger diameter 2-electrode designs, typically between 3 and 7 mm, are more applicable to the main discharge.

Micro-PPT propellant samples with 2 electrodes and different anode diameters were analyzed. These samples represent a fully charred, a partially charred and an uncharred Teflon surface. Microscopic analyses were performed on the Environmental Scanning Electron Microscope available at the EMAL Center at the University of Michigan. The sample chamber is held at a pressure of typically between 1-20 torr. The accelerating voltage is about 15-20 kV. X-ray Energy Dispersive Spectroscopy (XEDS) makes it possible to identify the chemical elements. Below we present some characteristic images taken from the fully charred sample.

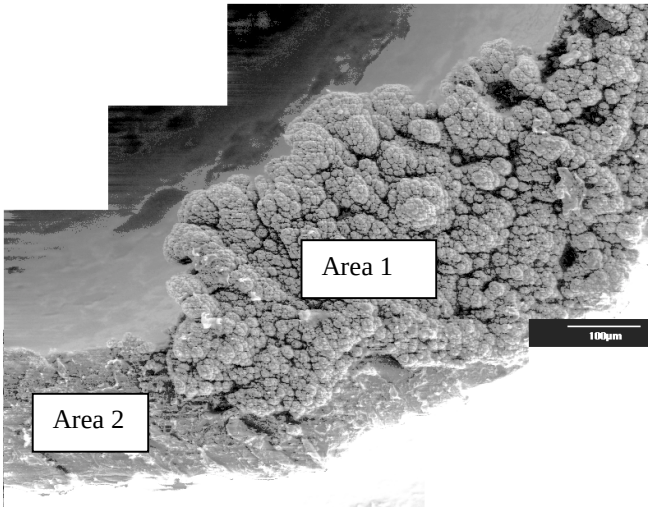

Figure 1. Charring area on the propellant surface of 3.6 mm micro-PPT

Generally two different structures are identified in the charred area (shown as Area 1 and Area 2 in Fig. 1) as can be concluded also from the high magnification images. One can conclude that Area 1 mainly contains Carbon and other small fractions of Fluorine, Copper (Cu), Silver (Ag) and Silicon (Si) as shown in Fig. 2. The images from Area 2 look very different as shown in Figure. 3. One can see that the main component here is Silicon. Small fractions of Cu and Ag are also found.

An analysis of the interface between Areas 1 and 2 as shown in Figure 1 suggests that the same structure (as in the image, Fig. 3) may lie under the Carbon charring. In order to verify this we removed the Carbon layer and analyzed the scratched area. We conclude from the element mapping that the scratched area contains Silicon as well as Fluorine.

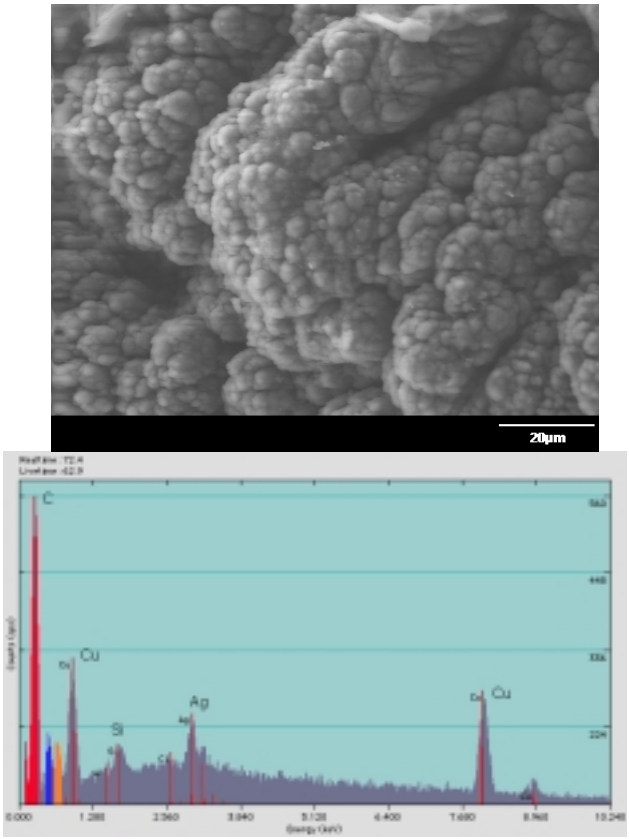

Figure 2. Image and XEDS results for the Area 1. The main peak corresponds to Carbon

Microscopic analyses of different fully and partially charred samples show that under the Carbon layer there is a layer of Silicon with some small amount of Copper. The origin of Copper is probably the outer electrode while Silicon may come from the diffusion pump or the vacuum facility.

In order to eliminate this possible source of Silicon the MicroPPT was fired in a chamber with a turbopump (glass bell jar). The image of this sample is shown in Fig. 4 and the typical image of the charred area is shown in Fig. 5.

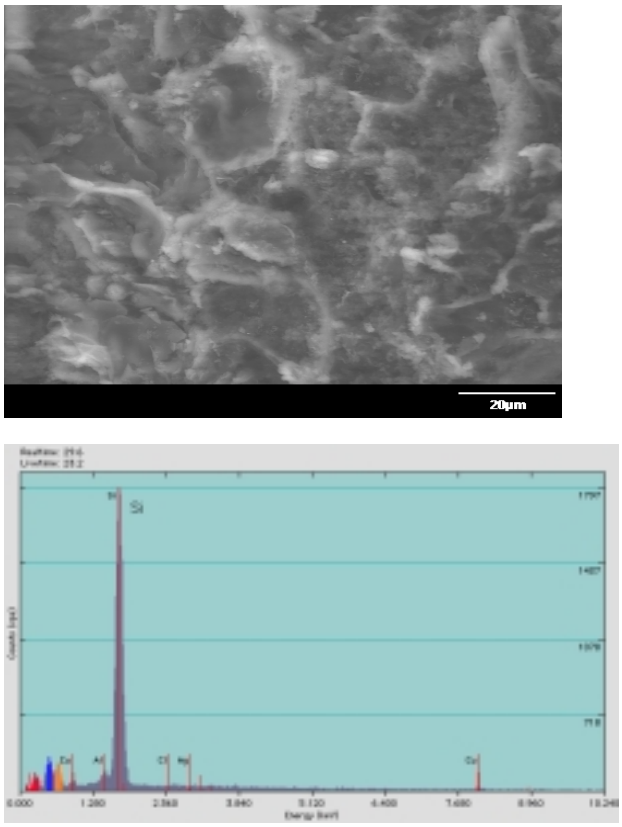

Figure 3. Image and XEDS results for the Area 2. The main peak corresponds to Silicon

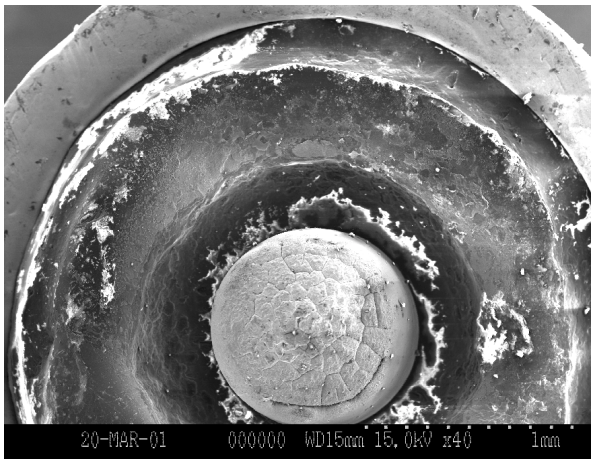

Figure 4. Propellant surface of 3.6 mm diameter micro-PPT

It is interesting to note that in the micro-PPT sample fired in the turbopumped chamber, there is no evidence of Silicon.

An important observation from the microscopic analyses is the presence in most samples of a layer of metal under the char. In those cases where no metal layer is found under the char, the charred area has the same appearance. It is concluded that the char formation therefore may be the same in both cases. This fact may suggest that the Carbon char is formed as result of the Carbon flux returned from the plasma rather than non-complete Teflon decomposition.

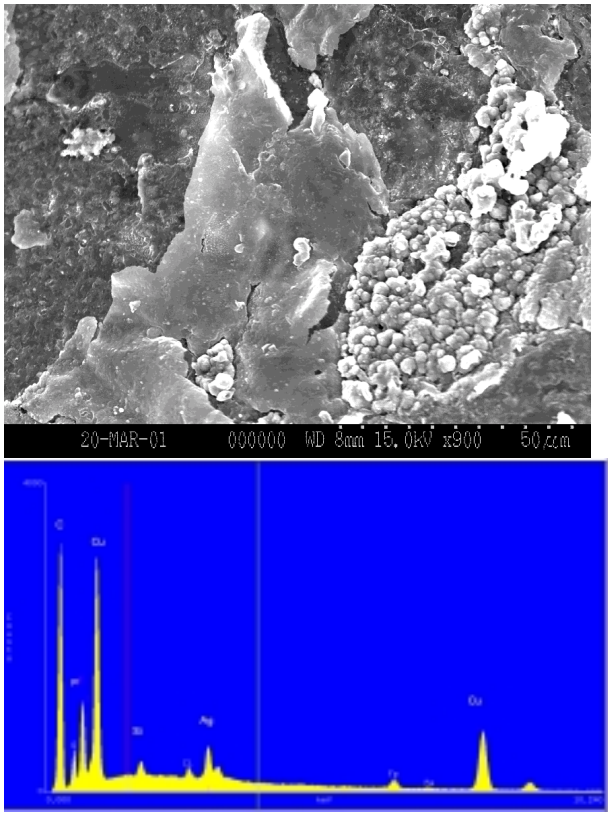

Figure 5. Charred area image and XEDS results. The main peaks corresponds to Carbon and Copper

Model

In this part we describe a model of the plasma layer near the evaporating surface with application to a micro-PPT that is shown schematically in Fig. 6.

The model includes the following features: Teflon ablation, plasma energy balance, heat transfer from the plasma to the Teflon, current spreading in the near field, and an equivalent RLC electrical circuit model. The Teflon ablation model is based on a recently developed kinetic ablation model.[12,13]

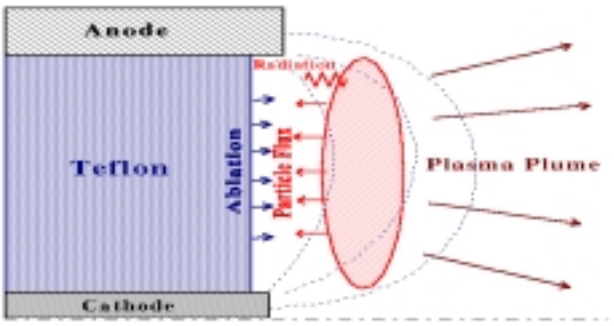

Figure 6. Schematic of the problem geometry and energy balance

The plasma energy balance and the heat transfer to the Teflon are based on a previously developed model of the ablation controlled discharge.[8,14] The energy balance in the layer has the following form:

$$3/2ndT/dt = Q_J - Q_r - Q_F \quad (1)$$

where n is the plasma density, T is the plasma temperature, Q_J is the Joule heat, Q_r is the radiation heat and Q_F is the energy flux due to particle convection. Mechanisms of energy transfer from the plasma column to the propellant bar include heat transfer by particle convection and by radiation. The inputs for the model are thruster geometry, Teflon material properties, and Teflon equilibrium pressure dependence on the surface temperature.

In the transition region between the plasma and the ablated surface, two different layers are distinguished: a kinetic non-equilibrium layer adjusted to the surface with a thickness of about one mean free path; and (2) a collision-dominated layer with thermal and ionization non-equilibrium. The solution for these two layers is coupled with the quasi-neutral plasma that allows the calculation of the ablation rate. The energy input in Eq. 1 depends upon the current density distribution near the ablated surface. In order to calculate the current density, the problem of the current distribution in the thruster near field is solved.

Current distribution in the plasma plume near field

Assuming that the magnetic field has only an azimuthal component and after neglecting the

displacement current, the magnetic field in the near field plasma plume is calculated from the magnetic transport equation in the following form:

$$\partial \mathbf{B}/\partial t = 1/(\sigma\mu)\nabla^2\mathbf{B} - \nabla\times(\mathbf{j}\times\mathbf{B}/en) + \nabla\times(\mathbf{V}\times\mathbf{B}) \qquad (2)$$

where σ is the plasma conductivity, μ is the permittivity, **j** is the current density and **V** is the plasma velocity.

A scaling analysis shows that the various terms on the right hand side of Eq. 2 may have importance in different regions of the plasma plume and therefore a general end-to-end plasma plume analysis requires keeping all terms in the equation. In the case of the near plume of the MicroPPT with a characteristic scale length of about 1 cm, the magnetic Reynolds number $Re_m<<1$ and therefore the last term can be neglected. Taking this into account in the dimensionless form, Eq. 2 can be written as:

$$Re_m\partial \mathbf{B}/\partial t = \nabla^2\mathbf{B} - (\omega\tau)\cdot\{\nabla\times(\nabla\times\mathbf{B}\times\mathbf{B})\} \qquad (3)$$

here $(\omega\tau)$ is the Hall parameter that measures the Hall effect. Therefore, depending on the plasma density, the Hall effect may be important for the magnetic field evolution.

Our estimations show that the Hall parameter $\omega\tau<<1$ if the plasma density near the Teflon surface $N>10^{23}$ m^{-3}. However, in general, the Hall parameter may vary for different devices and therefore in the future we will investigate the effect of the Hall parameter on the magnetic field distribution in the near field. From the magnetic field distribution the current density components can be calculated as follows:

$$J_r = - 1/\mu\ \partial B/\partial z$$
$$J_z = 1/\mu\ \partial B/\partial r$$

An example of the magnetic field distribution is shown in Fig. 7 for a 3.6 mm diameter propellant micro-PPT. The current density distribution is shown in Fig. 8. One can see that the thickness of the layer where the main part of the current is concentrated is about 1 mm from the Teflon surface. More details about the current and magnetic field distributions in the near field are presented in a recent paper[9].

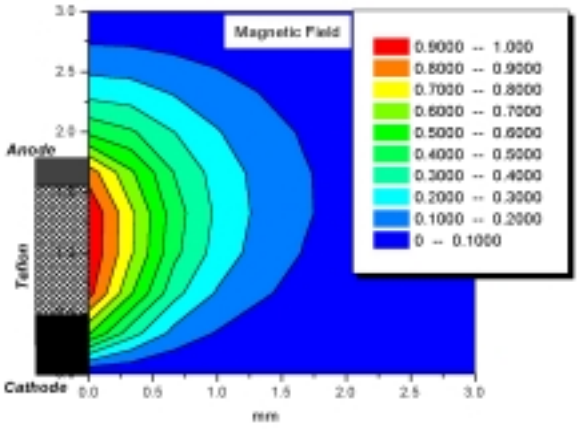

Figure 7. Magnetic field distribution in the near field of a 3.6 mm diameter micro-PPT

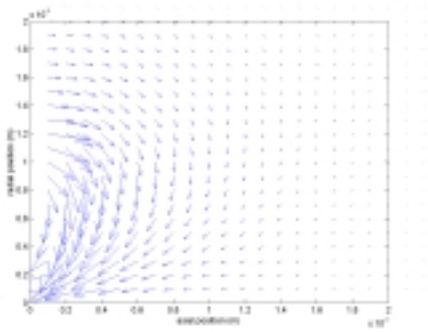

Figure 8. Current distribution in the near field of a 3.6 mm diameter micro-PPT

The current density radial distribution (according to Eqs. 2-4) near the Teflon surface is shown in Fig. 9.

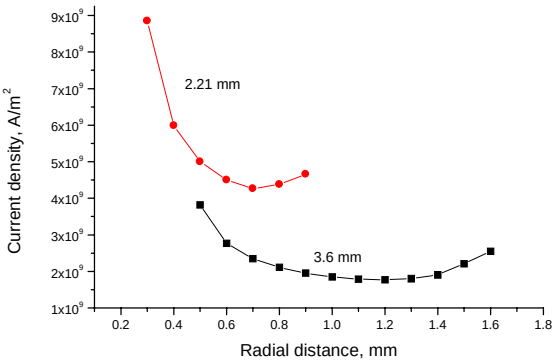

Figure 9. Current density near the Teflon surface

One can see that in the case of the smaller thruster (2.21 mm diameter) the current density is higher by a

factor of about 2 for the same total discharge current. The current density near the Teflon surface has a minimum due to the current spreading in r-z plane as shown in Fig. 8.

The dependence of the calculated ablated mass during the pulse is shown in Fig. 10 for two micro-PPT's with diameters of 3.6 mm and 2.21 mm.

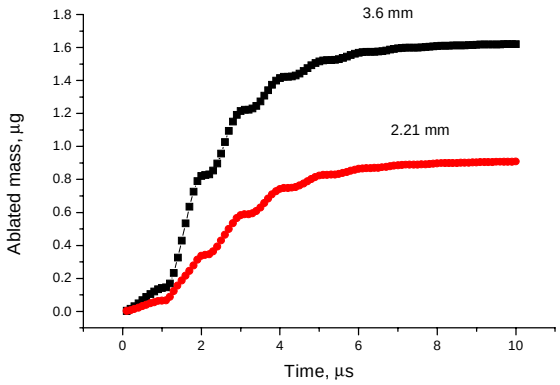

Figure 10. Ablated mass as a function of time with propellant diameter as a parameter

It should be noted that in the experiments, the average ablation mass was measured to be about 1.3 μg/shot in the case of the 2.21 mm diameter thruster. Our model predicts without any fitting parameter that the mass ablated per pulse is about 0.9 μg in this case. Taking into account that the late ablation in the form of macroparticles (that is not considered here but was observed in the micro-PPT[10]) may consume up to 40% of the mass[15], one can conclude that the model predicts the ablation rate reasonably well.

According to the energy balance (Eq. 1) and the heat transfer equation at the Teflon surface, the surface temperature should depend on the current density. The spatial and temporal variation of the Teflon surface temperature for the two thrusters is shown in Fig. 11. In these calculations, the experimental current waveform is used. In the case of the thruster with smaller diameter (2.21 mm), the Teflon surface temperature is higher by about 20 K and can be considered more uniform radially than that of the thruster with larger diameter during the whole pulse.

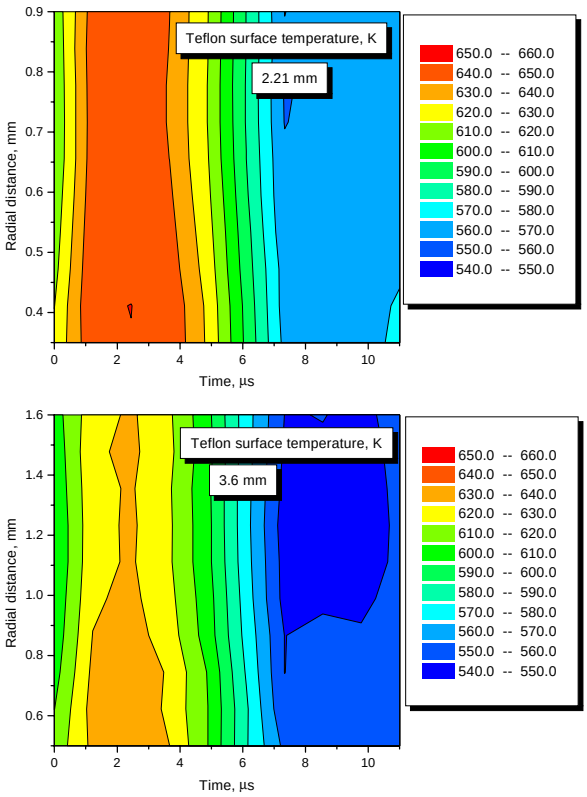

Figure 11. *Teflon surface temperature (K) temporal and radial variation for two MicroPPT designs with diameter 2.21 mm and 3.6 mm*

In the larger thruster (3.6 mm), the temperature has a minimum at radial distances of 1.1-1.3 mm. Since the Teflon ablation is approximately exponentially proportional to the surface temperature, the model predicts a lower rate of ablation in the areas where the surface temperature has a minimum. Taking this into account, the effect of the temperature distribution may be related to the preferential charring of the Teflon surface observed experimentally as shown in Fig. 12. It is interesting to note that comparison of the calculated temperature field and ablation rate with the photograph of the Teflon surface (see Fig. 12) shows that the area with surface temperature and ablation rate minimum corresponds to the charring area in the case of the 3.6 mm diameter thruster.

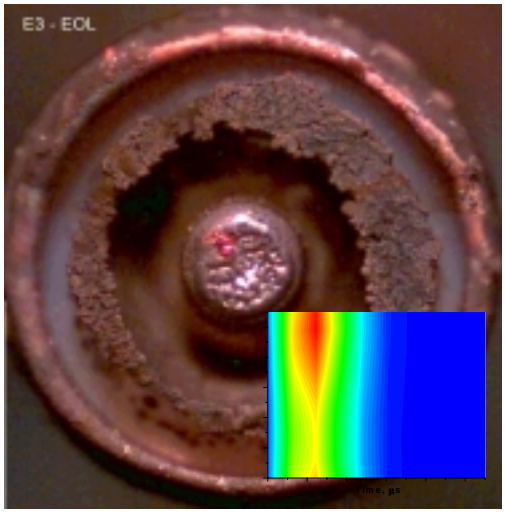

Figure 12. *Teflon surface photo (Ref. 6) and the Teflon surface temperature field and the ablation rate in the case of 3.6 mm diameter micro-PPT*

Effect of discharge energy

The current produced by an underdamped RLC circuit has the following form:

$$I(t) = I_p \sin(\alpha t)\cdot\exp(-\beta t)$$

where $\alpha=(1/LC - \beta^2)$, $\beta=R/2L$ and I_p is the current peak, $Ip=U_o/(L\alpha)$, where U_o is the initial voltage on the capacitor of capacitance C, R is the equivalent circuit resistance, L is the circuit inductance. From the comparison of I(t) with the experimental current waveform in the case of C=0.3 μF it is estimated that R=0.3 Ω and $L=3.6\cdot10^{-7}$ H.

We studied the effect of the discharge energy (CU_o^2) on the Teflon surface temperature and the Teflon ablation rate. These results are shown in Fig. 13. One can see that with the energy increase, the Teflon surface temperature and the ablation rate increase. These results suggest that increase of the discharge energy for constant capacitance leads to enhanced Teflon ablation.

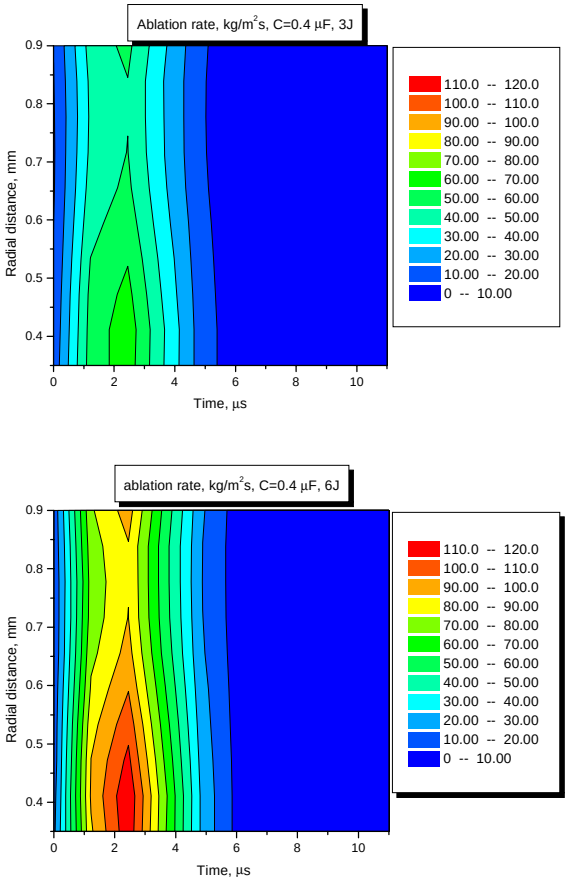

Figure 13. *Ablation rate temporal and radial variation for discharge energies of 3J and 6J.*

It was shown in experiment that the energy level affects the Teflon ablation. These experiments were conducted in the glass bell jar under a pressure of 10^{-6} torr. The char patterns for three different energies are shown in Fig. 14 after continuous firing for at least 8 hours and at 1 Hz. The cases with higher discharge energy were fired for longer duration to see if char would appear. There have been no experimental observations of cases where char appeared, only to be cleaned up by subsequent discharges at the same energy. (Cleaning of the char formation by firing at higher discharge energies has been observed experimentally, but is not considered within the context of this effort). For these tests a ¼" diameter 2-electrode MicroPPT was energized using a 0.417 uF capacitor. The charge voltage ranged from 2448V for the 1.25 J case, to 5364V for the 6 J case. Clearly

these voltages are insufficient to cause the surface breakdown needed for MicroPPT discharge initiation across a ¼" diameter. Rather than complicate the test setup by using the 3-electrode MicroPPT configuration[6], an auxiliary sparkplug, fired at 0.5 J, was used to initiate the discharge on command.

One can see that in the case of small energy, the charring in the area between the electrodes is observed while in the case of large energy, there is no charring. The middle energy case shows a level of char between the 2 extrema. This effect can be partially explained in terms of our model that shows that higher discharge energy leads to higher Teflon surface temperature

1.25 J, 1 Hz, 8 hrs **3 J, 1 Hz, 24 hrs** **6 J, 1 Hz, 72 hrs**

Figure 14. *Photo of the micro-PPT propellant surface for discharge energies of 1.25 J, 3J and 6J.*

Near field plume

In this section we will present measured and predicted electron density distributions in the near filed plume for one micro-PPT design. These data will be compared in order to verify our plume and device model.

Herriot Cell electron density measurement

An experimental basis for comparison is provided using a Herriott Cell interferometer. Electron density measurements are taken on a 6.35 mm (1/4") diameter MicroPPT at AFRL. The interferometer uses a single laser wavelength and quadrature heterodyne technique described by Spanjers *et al.*[16]

Addition of a Herriott Cell acts to confine a large number of laser passes into an area suitable for maximum exposure to the MicroPPT plume. This is achieved by focusing the laser between the two concave mirrors of the cell. The technique is used to increase signal-to-noise ratio for diffuse plasmas by increasing laser exposure to the plasma over a characteristic path length.[17] Thirteen laser reflections in the Herriott Cell were focused to two points, separated by 3 mm. For data shown here, these points formed a plane parallel to the fuel face and 5 mm distant. A schematic of the beam geometry is shown in Fig. 15.

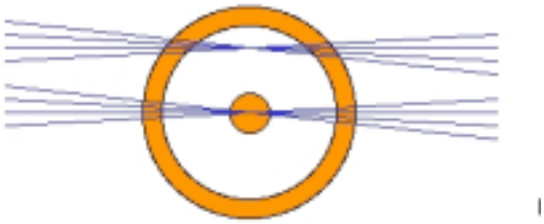

Figure 15. *Schematic showing interferometer coverage of the Micro-PPT fuel face using the Herriott Cell. The beams are situated 5mm from the propellant face.*

Figure 16 shows the experimental data from this geometry co-plotted with model predictions. The experimental data was taken at a discharge energy of 6.6 J from a 0.417 μF capacitor. Experimental waveforms of the current were obtained using a a self-integrating Rogowski coil. Peak density reaches $23\pm6\times10^{15}$ cm^{-3} with uncertainty due to shot-to-shot variations in thruster firing.

Near field plume simulations

Using the plasma layer model predictions as boundary conditions, we calculated the near field plume of the MicroPPT. This allows us to make direct comparison of our model predictions with measured data.

The general approach for the plume model is based on a hybrid fluid-particle approach that was used previously (Refs. 7). In this model, the neutrals and ions are modeled as particles while electrons are treated as a fluid. Elastic (momentum transfer) and non-elastic (charge exchange) collisions are included in the model. The particle collisions are calculated using the direct simulation Monte Carlo (DSMC) method[16]. Acceleration of the charged particles is computed using the Particle-In-Cell method (PIC)[17]. The ion dynamics is calculated by taking into account electromagnetic acceleration.

The electron dynamics is very important in the plasma plume of an electromagnetic PPT. Previously, our model was based on the assumption that electrons rapidly reach the equilibrium distribution and in the absence of a magnetic field can be described according to the Boltzmann distribution. While this was a satisfactory assumption in the case of an electrothermal thruster plume,[7] this is not suitable for the near field of an electromagnetic thruster. In the case of a magnetic field, the electron momentum equation reads (neglecting electron inertia):

$$0 = -e^2 n_e(\mathbf{E}+\mathbf{V}_e\times\mathbf{B}) - e\nabla P_e - \nu_{ei} m_e \mathbf{j}$$

The electric and magnetic field distributions in the plume are calculated from the set of Maxwell equations. More detailed study of the near field plume of the electromagnetic PPT was presented recently[9].

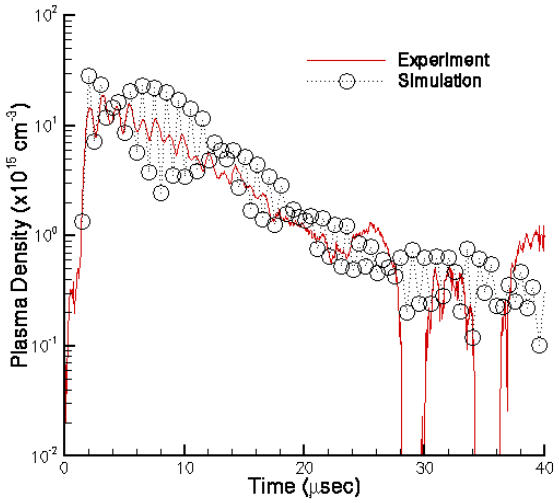

Figure 16. Comparison of predicted and measured electron density time variation at 5 mm from the propellant face at the axis in the case of 6.35 mm diameter micro-PPT firing at 6.6 J.

The calculated plasma density time variation at 5 mm from the propellant face at the axis is shown in Fig. 16. Plasma density peaks at about 3×10^{16} m^{-3} and decreases by few order of magnitude towards the pulse end. For comparison we show also measured plasma density (using Herriott Cell technique, see above section). One can see that our model correctly predicts both the plasma density level and temporal behavior during the entire pulse.

Summary

A model of the plasma layer near the Teflon surface of a PPT was developed that allows the calculation of the Teflon surface temperature and ablation rate self-consistently. It was found that the propellant size has an important effect on the Teflon surface temperature distribution and the ablation rate. For instance, in the case of the thruster with smaller diameter (2.21 mm) the Teflon surface temperature is higher by about 20 K and can be considered more uniform radially than that of the thruster with larger diameter during the whole pulse. In the larger thruster (3.6 mm), the temperature has a minimum at radial distances of 1.1-1.3 mm. The comparison of the temperature field and the ablation rate distribution with a photograph of the Teflon surface shows that the area with surface temperature and ablation rate minimum corresponds to the charring area in the case of the 3.6 mm thruster. This suggests that the charring may be related to the temperature effect. An analysis of the effect of the discharge energy E on the temperature distribution shows that the Teflon surface temperature and the ablation rate can be increased by increasing E. At the same time, the increase of capacitance leads generally to a smaller ablation rate, though this effect can be considered to be marginal.

A microscopic analysis of the charred areas showed that the charred area contained mainly Carbon. In some cases a metal layer was found under the Carbon char. The metal deposition is related to the electrode erosion while the Silicon is assumed to come from the diffusion pump. In fact, when a cryogen pumping system was used, no Silicon was obtained on the Teflon surface. In those cases where no metal layer was found under the char, the charred area has the same appearance. It is concluded that the char formation therefore may be the same in both cases. This fact may suggest that the Carbon char is formed as result of the Carbon flux returned from the plasma rather than non-complete decomposition of the Teflon.

Predicted electron density was directly compared with experimental data and very good agreement was obtained.

Acknowledgements

The first two authors gratefully acknowledge the financial support of the Air Force Office of Scientific Research through grant F49620-99-1-0040. The AFRL authors were also partially supported through the Air Force Office of Scientific Research with Dr Mitat Birkan as Program Manager.

REFERENCES

[1] R. L. Burton and P. J. Turchi, "Pulsed plasma thruster", Journal of Propulsion and Power, Vol.14, No. 5, 1998, pp. 716-735.

[2] R.J. Vondra and K.I. Thomassen, "Flight qualified pulsed plasma thruster for satellite control", *Journal of Spacecraft and Rockets*, Vol. 11, No. 9, 1974, pp. 613-617.

[3] P. J. Turchi, Directions for improving PPT performance, *Proceeding of the 25th International Electric Propulsion Conference*, vol. 1, Worthington, OH, 1998, pp. 251-258.

[4] E. Y. Choueiri, "System optimization of ablative pulsed plasma thruster for stationkeeping", *Journal of Spacecraft and Rockets*, Vol. 33, No. 1, 1996, pp. 96-100.

[5] R. A. Spores, R. B. Cohen and M. Birkan, "The USAF Electric propulsion program", *Proceeding of the 25th International Electric Propulsion Conference*, vol. 1, Worthington, OH, 1998, 1997, p.1.

[6] Spanjers, G.G., White, D., Schilling, J., Bushman, S., Lake, J., Dulligan, M., "AFRL MicroPPT Development for the TechSat21 Flight," 27th Intl Electric Propulsion Conference, IEPC paper 2001-166, Pasadena, CA 2001.

[7] I. D. Boyd, M. Keidar, and W. McKeon, Modeling of a pulsed plasma thruster from plasma generation to plume far field, *Journal of Spacecraft and Rockets, Vol. 37, No. 3, 2000.*

[8] M. Keidar and I.D. Boyd, "Device and plume model of an electrothermal pulsed plasma thruster", Paper AIAA-2000-3430.

[9] M. Keidar and I.D. Boyd, "Electromagnetic effects in the near field plume exhaust of a pulsed plasma thruster", AIAA Paper 2001-3638

[10] Gulczinski, F., Dulligan, M., Lake, J., and Spanjers, G.G., :Micropropulsion Research at AFRL," Paper AIAA-2000-3255.

[11] Antonsen, E., Burton, R., Spanjers, G.G., "*High Resolution Laser Diagnostics in Millimeter-Scale Micro Pulsed Plasma Thrusters*", 27th Intl Electric Propulsion Conference, IEPC paper 2001-157, Pasadena, CA 2001.

[12] M. Keidar, J. Fan, I.D. Boyd and I.I. Beilis, "*Vaporization of heated materials into discharge plasmas*", J. Appl. Phys., 89, 2001, pp. 3095-3098.

[13] M. Keidar, I.D. Boyd and I.I. Beilis, "*On the model of Teflon ablation in an ablation-controlled discharge*", J. Phys. D: Appl. Phys., 34, 2001, pp. 1675-1677.

[14] M. Keidar, I.D. Boyd and I.I. Beilis, "*Electrical discharge in the Teflon cavity of a coaxial pulsed plasma thruster"*, IEEE Trans. Plasma Sci., 28, 2000, p. 376-385.

[15] G.G. Spanjers, J.S. Lotspeich, K.A. McFall and R.A. Spores, "*Propellant losses because of particulate emission in a pulsed plasma thruster*", J. Prop. Power, 14, 1998, p. 554

[16] G.A. Bird, "*Molecular gas dynamics and the direct simulation of gas flows"* (Clarendon Press, Oxford, 1994).

[17] C.K. Birdsall and A.B. Langdon, Plasma Physics via Computer Simulation, Adam Hilger Press, 1991.

[16] G.G. Spanjers, K.A. McFall, F. Gulczinski III, R.A. Spores, "Investigation of Propellant Inefficiencies in a Pulsed Plasma Thruster, AIAA Paper 96-2723

[17] E.L. Antonsen, Herriott Cell Interferometry for Pulsed Plasma Density Measurements, MS Thesis, University of Illinois at Urbana-Champaign, 2001.